# Journal of Soil Sciences and Agricultural Engineering

Journal homepage & Available online at: www.jssae.journals.ekb.eg

# Remote Sensing and GIS Techniques for Irrigation Water Management in North Delta of Egypt under Water Scarcity Conditions

Zahem, N. E. \* : M. M. Ibrahim and Nadia G. Abd El-Fattah

Agricultural Engineering Department, Faculty of Agriculture, Mansoura University, Mansoura, Egypt;

ah Cross Marl



Article Information Received 15 / 9 /2025 Accepted 21 /10 /2025

# **ABSTRACT**

Remote sensing and GIS are effective for assessing crop water use and estimating evapotranspiration rates. This study aims to improve water management planning on selected farms by determining the best estimates of actual evapotranspiration (ETa). The selected site represents small-scale private farms located in the northern Nile Delta, Egypt. Using European Sentinel satellite images of the 2022-2023 periods, ETa values were estimated by three Remote Sensing (RS)-based models including the Surface Energy Balance Algorithm for Land (SEBAL), the Normalized Difference Vegetation Index-based method (ETa\_NDVI), and the Simplified Surface Energy Balance (SSEB). The efficiency of these models was compared using FAO-Penman-Monteith (FAO-P-M) as a reference model. The Penman-Monteith approach estimated the ETc to be 2.51, 3.81, 4.15, 3.84, 2.08, 2.06, 2.84, 7.52, 5.98, 5.07, 5.08 and 5.13 mm/day for wheat, clover, potatoes, sugar beet, flax, beans, onion, rice, maize, sesame, sunflower, and cotton respectively, whereas the estimated ETa from SEBAL for these crops were 2.24, 3.50, 4.06, 3.71, 2.08, 2.19, 3.10, 7.34, 5.74, 5.97, 5.14, and 5.37 mm/day respectively. The estimated ETa seasonal averages using ETa\_NDVI, SEBAL, and SSEB methods for wheat crop are 2.41, 2.43, 2.24 mm/day respectively. SEBAL achieved the highest R<sup>2</sup> value (0.96) and the lowest Root Mean Square Error (RMSE) (0.24 mm/day). In comparison, the ETa\_NDVI and SSEB models recorded R2 values of 0.74 and 0.85 with RMSE values of 0.79 and 0.65 mm/day, respectively. These results indicate that the SEBAL model is capable of reliably estimating ETa in selected farms, which can improve irrigation planning.

Keywords: Remote Sensing, SEBAL, Evapotranspiration, Egypt, Crops.

# INTRODUCTION

Water resources are undoubtfully one of the most important factors affecting agricultural production and sustainability (Ingrao et al., 2023). This is particularly true in water-scarce regions, such as the North Delta in Egypt, where population growth, economic development, and climate change are exacerbating pressure on water resources (MWRI, 2014; Chelkeba et al., 2023). The North Delta region of Egypt is characterized by intensive agriculture, with smallholder farmers relying on irrigation canals from the Nile River under arid climatic conditions (Lago-Olveira et al., 2023). Freshwater availability in this agricultural region is limited, which is critical given that agriculture relies heavily on the Nile River, which has recently been under increasing pressure due to water demands from various industries and urban expansion (Abdel-Shafy and Aly, 2002). The agricultural sector in Egypt is the largest consumer of water due to the most common irrigation system, flood irrigation, which consumes approximately 80% of water (Roushdi, 2024). Therefore, enhancing water use efficiency in agriculture is crucial to ensure food security and environmental sustainability (Kang et al., 2017). This can be achieved by the estimation of actual evapotranspiration (ETa), or crop water consumption. ETa represents water loss either from the surface of the soil by evaporation, or from the leaves of the plants by transpiration (Allen et al., 1998; Immerzeel et al., 2006; Senay et al., 2011). Estimating ETa is of great importance not only for improving the operation and management of irrigation systems, but also in the broader context of water resource management and strategy development (Raza et al., 2023).

Several on-field methods exist for direct measurement of ETa including the lysimeter system (Pruitt and Angus, 1960), and eddy covariance flux towers (Swinbank, 1951). Indirect measurement of ETa can be achieved using evaporation pans (Snyder, 1992), and Bowen's ratio (Fritschen, 1965). Despite being accurate, these point measurements are limited to time and place (Al Zayed *et al.*, 2016) and are based on gathered meteorological data which is still a difficulty in poor regions (El-Shirbeny *et al.*, 2015).

Remote sensing (RS)-based methods, on the other hand, are vital for monitoring ETa at spatiotemporal scales (Immerzeel et al., 2006; Al Zayed et al., 2016; El-Shirbeny et al., 2015). RS and geographic information systems (GIS) technologies provide an efficient means of collecting and analyzing massive amounts of spatial and temporal data, thus providing a more integrated view of irrigation water use patterns over large and diverse areas, evapotranspiration levels, and irrigation efficiency for various agricultural fields (Baban, 2022; Ali and Khedr, 2018). Thus, the application of remote sensing RS techniques to estimate ETa is useful when field measurements are expensive or unavailable and smallholders with mixed cropping systems are prevalent (Folhes et al., 2009).

There are many RS models that can estimate ETa, Surface Energy Balance Algorithm for Land (SEBAL) and Simplified Surface Energy Balance (SSEB) are two of them and they are used to estimate ETa (Losgedaragh and Rahimzadegan, 2018). Also, Normalized Difference Vegetation Index (NDVI)-based model (ETa\_NDVI) can estimate ETa by calculating crop coefficient which is correlated to NDVI (Elsayed *et al.*, 2022). The SEBAL method relies on the surface energy balance to calculate actual evapotranspiration. The model is based on remote sensing

\* Corresponding author. E-mail address: naderzahim123@gmail.com DOI: 10.21608/jssae.2025.423795.1317 data applied from satellite images covering the assessment of various heat fluxes developed in terrestrial systems (Sun et al., 2011). This model does not require a large amount of ground data, making it effective in areas where meteorological stations are not available in terms of cost or time (Fawzy et al., 2021). On the other hand, SSEB is a simplified approach to SEBAL, as it is based on the concept of surface temperature using temperature differences from thermal infrared satellite data, which determines evaporative water loss between surface types due to energy differences (Wagle et al., 2017; Sebbar et al., 2024). The accuracy of SSEB results was shown to be close to that of SEBAL using less input (Savoca et al., 2013; Senay et al., 2011). The Food and Agriculture Organization Penman-Monteith model (FAO-P-M) is a wellknown and reliable method for estimating reference evapotranspiration (ETr), which is one of the accepted models in the scientific community and is recommended by the FAO (Penman, 1948; JL, 1965; Allen et al., 1998). It combines several climatic factors: solar radiation, maximum and minimum air temperatures measured at meteorological stations, as well as wind speed and relative humidity (Sentelhas et al., 2010).

Several studies have applied RS-based methods to estimate ETa at different spatial scales in Egypt, including at the national level (Abdel Kader *et al.*, 2015), in the Nile Delta (Elhag *et al.*, 2011; El-Shirbeny *et al.*, 2014; Ayyad *et al.*, 2019; Elnmer *et al.*, 2019; Omar *et al.*, 2019; Fawzy, 2021), and on small-scale agricultural farms (Elsayed et al., 2022). Their studies relied on evapotranspiration estimation algorithms such as SEBAL, SSEB, and the ETa\_NDVI, among others, to accurately estimate ETa in Egypt. Most previous studies have been conducted, to some extent, at broad scales ranging from subnational to national and regional levels. However, spatial and temporal analysis of ETa at the small-scale, farm-level is scarce (Foster *et al.*, 2019).

Furthermore, it is worth noting that the Nile Delta region is also highly subdivided. Most farms are small (often <2 ha), and fields have been successively split by inheritance and expanding towns (Alfiky *et al.*, 2012; Rihan, 2024). This is known to hinder productivity and efficiency, as small farms are harder to mechanize. This understanding of small-scale irrigation consumption is essential for improving agricultural water management, particularly in arid and semi-arid regions where irrigation water is scarce (Deng *et al.*, 2006). Because ground surveys cannot easily track thousands of small farms,

RS and GIS have become indispensable. However, their suitability for spatial and temporal analysis of ETa at small-scale farms, especially in arid regions, is yet to be put into test (Foster *et al.*, 2019).

This study presents a new approach by combining SEBAL, SSEB and NDVI models using Sentinel-2 and Sentinel-3 data within a GIS environment to provide the most accurate estimate of actual evapotranspiration (ETa) at 10 m spatial resolution in Egypt.

Therefore, this study aims to compare the efficiency of three RS and GIS techniques in estimation of ETa for various crops on selected farms in the North Nile Delta region of Egypt. This is achieved by applying three ETa-estimating models: SEBAL, ETa\_NDVI, and SSEB, and comparing with FAO-P-M as a reference model. This study is expected to improve water resource management on selected farms in this region by selecting the best remote sensing model to estimate irrigation water consumption in such situations. This can enhance irrigation efficiency, reduce water waste, and increase agricultural productivity under harsh climatic conditions and water scarcity. It will also provide essential insights for decision-makers to develop more efficient and sustainable irrigation policies.

# MATERIALS AND METHODS

# 1. Study Area and Data Source Study Area

The geographical area to be studied is located in the northeastern part of the Nile Delta, within the borders of Dakahlia Governorate, Arab Republic of Egypt (31.10–31.18° N, 32.00–32.07° E). The area includes agricultural lands for small farmers, and its water is drawn from four canals branching off from the fifth branch of the Salam Canal known as "El Gannabeya El khamisa" (the fifth parallel canal in Arabic) and managed by the Salam Irrigation Engineering Department of the Ministry of Irrigation and Water Resources. The four climatic seasons in this area are characterized by mild winters and hot summers.

The study area has a surface water network that includes numerous streams and artificial waterways that the government is working to line in the study area. Figure 1 illustrates the geographical location of the study area and its latitude and longitude.

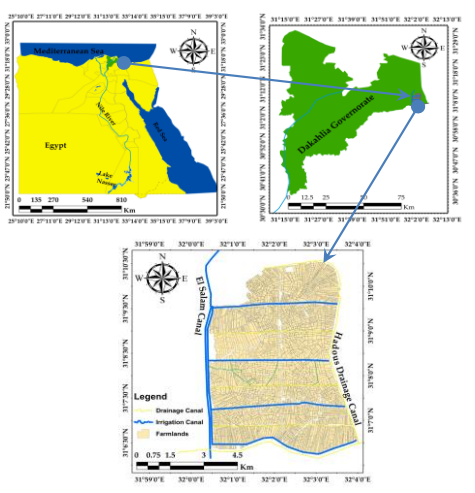


Figure 1. Illustrative map of the study area in North Delta Egypt (Geographical location).

#### Weather Data

The climate data used in this study were obtained from NASA's POWER website using the Power Data Access

Viewer version 2.0.0 (https://power.larc.nasa.gov/data-access-viewer/) for Dakahlia Governorate, Egypt.

These data were tabulated to estimate the daily reference evapotranspiration rate (ETr) for the image day.

Also, the daily humidity data such as vapor pressure or dew point temperature were used to complete the ETr calculations. **Image Dataset and Preprocessing** 

Satellite images were selected for this study based on their suitability for crop classification and effective ETa estimation. Freely available Sentinel-2 images, comprising 12 spectral bands, were used as the primary data source for this study (as detailed in Table 1). Four of these bands (Blue, Green, Red, and Near-Infrared) offer a spatial resolution of 10 meters which is sufficient for detailed vegetation analysis. Sentinel 2 images also have high temporal frequency as the average revisit time for Sentinel-2 satellites over the study area is approximately five days. Cloud-free Sentinel-2 images covering the study area were downloaded from the official Copernicus (https://scihub.copernicus.eu/) operated by the European's union.

We also used Sentinel-3 Level 2 lands surface temperature (SL\_2\_LST) thermal data (https://sentinel.esa.int/web/sentinel/user-guides/sentinel-3-slstr/product-types/level-2-lst). They are acquired by the Sea and Land Surface Temperature Radiometer (SLSTR) sensors onboard Sentinel-3A and 3B satellites. These data are processed by the European Space Agency (ESA) and presented at a nominal spatial resolution of 1 km. Sentinel-3 mission offers high temporal resolution, with revisit intervals of less than one day, ensuring continuous monitoring capability for land surface temperature dynamics.

The combination of Sentinel-2 and Sentinel-3 datasets provided a balanced integration of high spatial detail and frequent temporal coverage, fulfilling the essential requirements for the intended agricultural and environmental analyses.

Table 1. Technical specifications of the Sentinel-2 satellites

Satellites -		Sentine	Launched	Launched in June 2015 Launched in March 2017					
Satemies -		Sentine	Launched in						
Sensing instrument			ment (MSI)						
Swath width	290 km								
Temporal resolution	5 days (at equator)								
_	Band(ρ)(No.)	Central wavelength( $\lambda$ )(nm)	Spectral width( $\Delta\lambda$ )(nm)	Region	Spatial resolution(m)				
_	1	443	20	Coastal aerosol	60				
	2	490	65	Blue	10				
	3	560	35	Green	10				
	4	665	30	Red	10				
	5	705	15	Vegetation red edge (VRE)	20				
Spectral and spatial	6	740	15	Vegetation red edge (VRE)	20				
resolution	7	783	20	Vegetation red edge (VRE)	20				
	8	842	115	Near-infrared (NIR)	10				
	8a	865	20	Narrow NIR	20				
	9	940	20	Water vapour	60				
	10	1375	30	Short wave infrared (SWIR) cirrus	60				
	11	1610	90	SWIR	20				
	12	2190	180	SWIR	20				

# 2. Technical Process Software Used

Several geographic information systems (GIS) and image processing applications were used in this study to greatly facilitate the work. The Sentinel Application Platform (SNAP) version 9.0 was designed by the European Space Agency (ESA) to efficiently display, analyze, and process Sentinel satellite data. Zip-formatted satellite data can be read directly into SNAP without the need for extraction. Furthermore, the mosaic process in SNAP does not require stacking 2 image layers, saving time. SNAP was used for resampling, segmenting areas of interest, and extracting vegetation indices.

In addition, ArcGIS version 10.8 was used to digitize the boundaries of the study area (North Delta, Egypt), and the Boundary Tool was used to crop the study area image. Meanwhile, CROPWAT version 8.0 was used to estimate reference evapotranspiration using the FAO Penman-Monteith model.

#### Research Process

The main crops in the study area have a large and diverse area and clear boundaries. The specific experimental process is illustrated in Figure 2 for estimating  $\mathrm{ET}_a$  from different methods using Sentinel images.

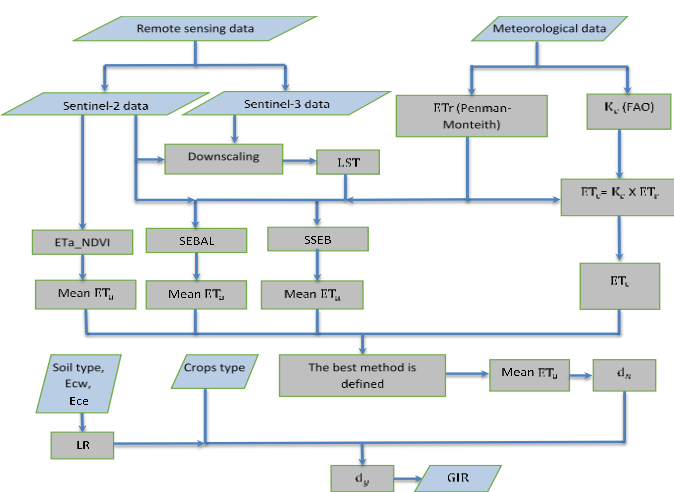


Figure 2. The flowchart of methodology followed.

# Estimation of Reference Evapotranspiration (ETr)

ETr is computed using the FAO-Penman-Monteith equation on a 24-hour time scale for the studied dates (Allen *et al.*, 1998). The computed ETr values are used to establish actual evapotranspiration (ETa) in this study area. ETr value is determined using the following formula:

$$ETr = \frac{0.408 \Delta (R_n - G) + \gamma \frac{900}{7 + 273} u_2(e_s - e_a)}{\Delta + \gamma (1 + 0.34 u_2)}$$
 (1)

Where; ETr Reference evapotranspiration (mm/day),  $R_n$  Net radiation at the crop surface (MJ.  $M^2$ .day¹), G Soil heat flux density (MJ.  $M^2$ .day¹), T Mean daily air temperature at 2 m height (°C),  $u_2$  wind speed at a height of 2 meters from agricultural fields (m/s),  $\gamma$  Saturation vapor pressure (kPa),  $e_a$  actual vapor pressure (kPa),  $e_s - e_a$  Saturation vapor pressure deficit (kPa),  $\Delta$  Slope vapor pressure curve (kPa/°C),  $\gamma$  Psychometric constant (kPa/°C).

### **Description of the Remote Sensing Methods Used**

Actual evapotranspiration cannot be obtained directly from satellite imagery, but it can be estimated based on surface radiation models using empirical remote sensing methods. The methods used, SEBAL, SSEB, and ETa\_NDVI, are explained in detail below.

# Surface Energy Balance Algorithm for Land with Sentinel-2 (SEBAL)

SEBAL calculates instantaneous evapotranspiration flux  $(ET_{inst})$  from satellite imagery and weather data using an energy balance equation without information on soil, crops, and management practices. It is important to use a clear sky image, as thin cloud layers can introduce significant errors in the calculations. Cloud free images result in accurate land surface temperature maps.

The algorithm calculates ETa through a series of calculations that estimate net surface radiation  $(R_n)$ , soil heat flux (G), and sensible heat flux (H) to the air using satellite imagery and meteorological data. The ETa flux is then calculated as a residual value of the surface energy balance equation.

The basic equations of the algorithm can be described, but detailed equations can be found in (Bastiaanssen *et al.*, 1998)

Figure 3. illustrates the computational steps for calculating ETa using the SEBAL algorithm.

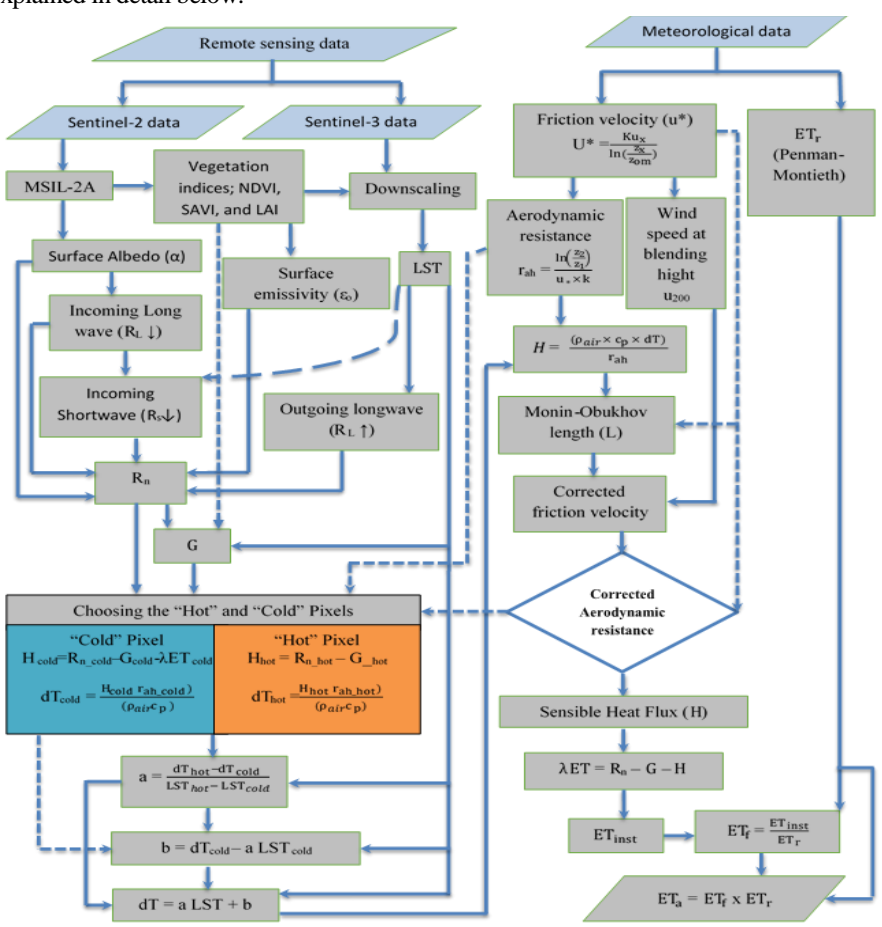


Figure 3. Flowchart of the methodology used in SEBAL model.

Instantaneous latent heat flux ( $\lambda$ ET) is calculated as the residual of the energy balance as illustrated in equation (2). The ratio of  $\lambda$ ET to ETr provides the evaporative fraction (ETf), which is used to scale the instantaneous ET to daily ETa.

$$\lambda ET = R_n - G - H \qquad ((2)$$

Where;  $\lambda$ ET the latent heat flux (watt/m²),  $R_n$  the net radiation flux at the surface (watt/m²), G the soil heat flux (watt/m²) and H the sensible heat flux to the air (watt/m²). The net radiation flux  $(R_n)$  is estimated using the following equation:

$$R_u = (1-\alpha) R_L \downarrow + R_L \downarrow - R_L \uparrow - (1-\epsilon_0) R_L \downarrow$$
 (3)

Where;  $\alpha$  the canopy reflection coefficient or Surface Albedo (dimensionless),  $\epsilon_{\sigma}$  the surface emissivity (dimensionless),  $R_{s}\downarrow$  the incident shortwave radiation  $(W/m^{2})$ ,  $R_{L}\uparrow$  the outgoing long wave radiation from the surface  $(W/m^{2})$  and  $R_{L}\downarrow$  the incident long wave radiation to the surface  $(W/m^{2})$  (Li *et al.*, 2013). In this study, the surface albedo  $(\alpha)$  was calculated using the corrected radiance of Sentinel image.

The G/Rn ratio is calculated using the following equation, which represents values near midday. The G ratio is also calculated by multiplying G/Rn by the Rn value in the ArcGIS Model Builder (Bastiaanssen, 2000).

# $G/R_0 = \alpha \times LST (0.0038 + 0.0074 \alpha) (1 - 0.98 NDVI^4)$

Where; LST refers to the surface temperature (°K), a represents the surface albedo, and NDVI the normalized difference vegetation index.

Surface reflectance ( $\alpha$ ) is theoretically defined as the ratio of the spectrally integrated reflected solar radiation to the incident solar radiation across the shortwave band (0.4 - 2.4 μm) as in equation (5). This definite integral is approximated by a weighted sum over the Sentinel-2 data bands. It is calculated as in equation (6).

$$\alpha = \frac{\int_{LO_{bl}}^{UP_{bl}} R_{s\lambda} d\lambda}{\int_{0.4}^{2.4} R_{s\lambda} d\lambda}$$
 (5)

$$\alpha = \sum_{bi} |\rho_{bi}.\omega_{bi}|$$
 (6)

Where;  $R_{si}$  extra-terrestrial irradiance for wavelength  $\lambda$  ( $\mu$ m),  $UP_{ti}$  and  $LO_{ti}$ are upper and lower wavelength bounds for Sentinel-2A band b, respectively.  $\rho_{bi}$  the surface reflectance in the spectral band (b<sub>i</sub>) from the Sentinel-2 (Level 2A) data, and bi represents the weighting factor for that band.

For a given band  $b_i$  in Level 2A Sentinel-2,  $\omega_{bi}$  the weighting factor that represents the fraction of the solar radiation derived from the solar radiation spectrum within the spectrum for the bi bands as shown in Table 2, where it was calculated for Sentinel-2A and Sentinel-2B from ESUN data. These selected bands were used specifically because they cover the most important spectral regions that influence the reflectance of soil and vegetation. They are divided into three groups. The first is visible light (VIS), represented by bands 2, 3, and 4, which is important for determining the color of surfaces such as soil, water, plants, etc. The second is nearinfrared (NIR), represented by bands 5, 6, 7, and 8. Its importance lies in its sensitivity to vegetation, as vegetation reflects NIR significantly, while soil and water reflect less. The final group is short-wave infrared (SWIR), represented by bands 11 and 12. Its importance lies in its sensitivity to soil and plant moisture, mineral composition, and changes in surface structure and properties that are not apparent in the visible or NIR.

Sensible Heat Flux (H) is computed according to the following equation:

$$H = \frac{(\rho_{air} x c_p x dT)}{r_{ab}}$$
(7)

Where;  $\rho_{air}$  the air density (1.25 kg/m<sup>3</sup>), Cp the specific heat of the air (J/kg. °K), dT the difference in temperature (T1-T2) between two heights  $(Z_1 \text{ and } Z_2)$  respectively (°K), and  $r_{ah}$  the aerodynamic resistance to heat transport (s/m) (Li et al., 2013).

Table 2. Weighting coefficients for calculating albedo in the SEBAL algorithm used in equation (6).

Band	Central wavelength Spectra		ctralwidth Sentinel-2A			Sentinel-2B		
<u>(ρ)</u>	(λ)	$(\Delta\lambda)$	Esun	ω <sub>bi</sub>	Esun	ω <sub>bi</sub>		
(No.)	(μm)	(μm)	(Wm <sup>-2</sup> / μm)	(-)	(Wm <sup>-2</sup> / μm)	(-)		
1	0.443	0.020	1874.3	N/A	1874.3	N/A		
2	0.490	0.065	1959.75	0.1346	1959.75	0.1344		
3	0.560	0.035	1824.93	0.1252	1824.93	0.1252		
4	0.665	0.030	1512.79	0.1038	1512.79	0.1038		
5	0.705	0.015	1425.78	0.0978	1425.78	0.0978		
6	0.740	0.015	1291.13	0.0884	1291.13	0.0886		
7	0.783	0.020	1175.57	0.0798	1175.57	0.0806		
8	0.842	0.115	1041.28	0.0715	1041.28	0.0714		
8a	0.865	0.020	953.93	N/A	953.93	N/A		
9	0.940	0.020	817.58	N/A	817.58	N/A		
10	1.375	0.030	365.41	N/A	365.41	N/A		
11	1.610	0.090	247.08	0.0169	247.08	0.0169		
12	2.190	0.180	87.75	0.0059	87.75	0.0060		
ΣESUN			14561.84		14577.28			

Note: The eight bands used to estimate  $\alpha$  (albedo) in SNAP are highlighted in bold and N/A = not used in SEBAL reflectance calculation.

# Simplified Surface Energy Balance (SSEB) Algorithm

It is simpler than the SEBAL algorithm, requiring only the average temperatures of hot and cold pixels to solve the energy balance equation to derive evapotranspiration. The

following equation is used to calculate 
$$ET_a$$
:
$$ETa = ET_f \cdot ET_r \quad (8)$$

$$ET_f = \frac{T_{hot} - LST}{T_{hot} - T_{cold}} \quad (9)$$

Where: ET, the evapotranspiration fraction from hot and cold pixels (dimensionless), ETr the reference evapotranspiration rate (mm/day), T<sub>hot</sub> the temperature of hot pixels, LST the ground surface temperature, and  $T_{cold}$  the temperature of cold pixels.

# ETa\_NDVI Method

The method implies the derivation of the crop coefficient (K<sub>c</sub>) like that of the Simplified Surface Energy Balance (SSEB) method and is therefore classified as one of the spectral vegetation indices approaches.

The Sentinel-2 imagery ensures mapping of ETa through the spectral data that is crucial for crop coefficient estimation. Sentinel-2 images calculate ETa NDVI using the following equations:

$$ETa\_NDVI = K_{c max} (1 - WDI) ETr$$
 (10)

$$ETa\_NDVI = K_{c max} (1 - WDI) \underbrace{ETr}_{C max} (10)$$

$$WDI = \frac{LST - T_{wet}(NDVI)}{T_{dry}(NDVI) - T_{wet}(NDVI)} (11)$$

Where; K<sub>cmax</sub> maximum K<sub>c</sub> value for the dense plants equal 1.2 (dimensionless), ETr reference evapotranspiration (mm/day), WDI water deficit index and is estimated from LST as shown in equation (11), LST earth's surface temperature ( ${}^{o}K$ ),  $T_{wet}$  lowest temperature at each NDVI, T<sub>drv</sub> highest temperature at each NDVI, NDVI the normalized difference vegetation index. The term (1 - WDI) in equation (10) is neglected if its size is small.

## Validation and Evaluation of Remote Sensing Methods

Prior to implementing remote sensing models such as SEBAL, all input datasets, whether meteorological or satellite imagery, were thoroughly verified to ensure consistency and spatial accuracy. Sentinel images were examined for cloud contamination, particularly in the northern Nile Delta, and post-processing steps were performed. Additionally, the selection of hot and cold pixels anchored using ground-based GPS reference points and visual inspection were performed to ensure accurate representation of harsh surface conditions.

To validate the ETa derived from the various remote sensing techniques employed in this investigation, the ETc produced by the FAO-P-M approach was utilized. The relationship between ETc values estimated using the FAO-P-M technique was compared with SEBAL, SSEB, and ET<sub>a</sub> NDVI using the coefficient of determination (R<sup>2</sup>). Additionally, the difference between the ETa values produced by the various algorithms and those determined by the FAO-

P-M technique was measured using the root mean square error (RMSE) as follows:

RMSE = 
$$\sqrt{\sum_{i=1}^{N} \frac{(S_i - O_i)^2}{N}}$$
 (12)

Where;  $S_i$  measured ETa by SEBAL, SSAB and ETa\_ NDVI algorithm (mm/day),  $O_i$  estimated ETa by FAO P-M (mm/day), and N the number of observations.

#### Land Use and Land Cover Analysis

A comprehensive field survey was carried out across the study area, accompanied by an analysis of land use and land cover to assess spatial and temporal variations in land use patterns and to estimate the cultivated areas for each crop type. Satellite images were used to process and interpret the data using spectral analysis and supervisory classification techniques. The images were geometrically and radiometrically corrected before classification to ensure the accuracy of the results.

A Global Positioning System (GPS) tool was then used to obtain accurate data for the location points for each of the different cultivated land type classes used in the classification process.

The Random Forest (RF) method, using the SNAP software, was used to classify the different images. RF classification is widely used in remote sensing for image classification (Peng *et al.*, 2022, Billah *et al.*, 2023). Classification accuracy was verified using reference data from field visits, calculating the error matrix and Kappa coefficient value.

The accuracy of the classified images was assessed using 30% of the collected land class points, while 70% was used to train the model. Visual interpretation of satellite imagery, supported by field observations, was also used to validate land use maps.

This analysis helped produce updated maps showing the spatial distribution of different categories, such as areas planted with wheat or other crops, providing a solid basis for assessing environmental changes, defining areas, and planning sustainable land use.

# Calculating Gross Irrigation Water Depth $(d_g, mm)$

According to (Döll and Siebert, 2002),  $d_g$  the entire amount of water applied to a field during irrigation, including water wasted as a result of inefficiencies such as evaporation, runoff, and deep percolation.

$$d_g = \frac{d_n}{\frac{E_0}{100}}$$
 (if  $L_R \le 0.1$ ) (13)

$$d_g = \frac{d_n}{\frac{E_n}{E_n}(1 - L_R)}$$
 (if  $L_R > 0.1$ ) (14)

Where;  $d_g$  gross irrigation water depth (mm),  $d_n$  net irrigation water depth (mm) on day i, and  $E_a$  field application efficiency = 55% based on assumption according to (Eisenhauer *et al.*, 2021).

### Calculating Crop Gross Irrigation Water Requirements (GIR, m<sup>3</sup>)

The area of every crop (feeds) or percentage of the canal's served area was entered manually to the crop's manipulation tool. GIR is calculated for all ON times throughout the year based on the original Standard:

$$\textit{GIR} = \frac{d_g \times A_c \times 4200}{1000} \qquad (15)$$

Where; GIR gross irrigation water requirements for crop  $(m^3)$ , and  $A_c$  the area of crop that's entered to the module, based on land use and land cover analysis.

# Canal Available Water Amount (CAW, m<sup>3</sup>)

CAW is the total amount of water that will be carried on the canal during ON time. CAW was calculated for all rotations ON time periods throughout the year according to the following equation:

$$CAW = Q_f \times A_f \times L_{on} \qquad (16)$$

Where;  $Q_f$  amount of water determined for feddan (m³) is 45 m³/feddan/day, based on the assumption according to the ministry of water resources and irrigation,  $A_f$  canal served area (feddan), and  $L_{on}$  length of time period of rotation (day).

# RESULTS AND DISCUSSION

# 1. Resulted Reference Evapotranspiration (ET<sub>r</sub>) using FAO-P-M

Figure 4 illustrates the maximum temperature (Tmax) and minimum temperature (Tmin) while Figure 5 rainfall wind speed and ETr. The maximum temperature (Tmax) experienced a range of nearly 20 °C in the winter months to peaking in summer at around 38 °C (in July). The Tmin ranged from 9.4 °C to 24.5 °C during this period, correlating with previous climatological studies in the northern part of the Nile Delta, which indicated a strong variability of seasonal temperatures (Sayad et al., 2016). The ETr observed in the study area varied from 1.5mm/day to 8.4mm/day. The ETr value appeared lowest on December 29, 2022, while the highest ETr value appeared on June 28, 2023; the observed patterns of seasonal reference ETr (low ETr in winter and high ETr in summer) have been reported in the Nile Delta and by areas close to Egypt and the mid-latitudes (Abou El Hassan, 2011). Across the annual timeframe, precipitation was mostly low and non-systematic with distinct increases in the winter months that corresponds to the rainfall pattern and variability that aligns with the regional precipitation trend research conducted over the Nile Basin and Delta (Balataa et al., 2024). The graph also reveals that the wind speeds were mostly within the range of 2-6 m/s, despite some sudden increases happening as well. The semi-arid characteristics of the climate prevailing over the Nile Delta reflect the requirements of crops for water to satisfy temperature high in summer and high evapotranspiration. Rainfall is insufficient to compensate for water losses thereby increasing dependence on irrigation water (El-Din, 2013).

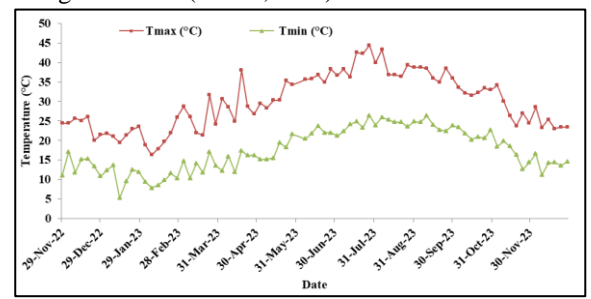


Figure 4. Maximum and minimum temperatures in the northern delta at the study area in the 2022-2023 periods.

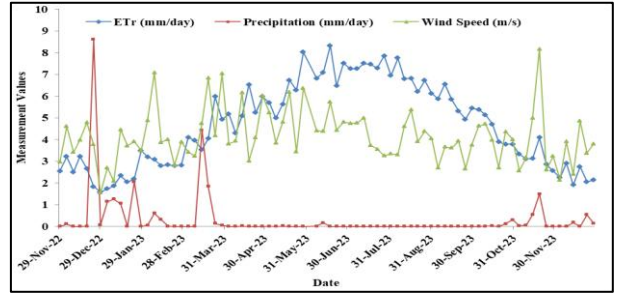


Figure 5. Evapotranspiration (ETr), Precipitation and wind speed in the northern delta at the study area in the period 2022-2023.

# 2. Spatial and Temporal Distribution of Actual Evapotranspiration in the Study Area

The maps of actual evapotranspiration (ETa) estimated from the SEBAL, SSEB, and ETa\_NDVI models are presented in Figure 6. The dark blue areas show regions of high ETa values corresponding to intense vegetation and irrigated agricultural lands, whereas the orange areas show regions with relatively lower ETa values generally associated

with built-up and barren lands. This spatial pattern reflects the very well-developed connection between vegetation density, surface moisture content, and Keith's ETa values associated with transpiration. Similarly, (El-Shirbeny *et al.*, 2021; Elbeltagi *et al.*, 2021), observed similar patterns of ETa with higher values over agricultural areas compared to urban or barren lands in the context of semi-arid conditions in the Nile Delta region.

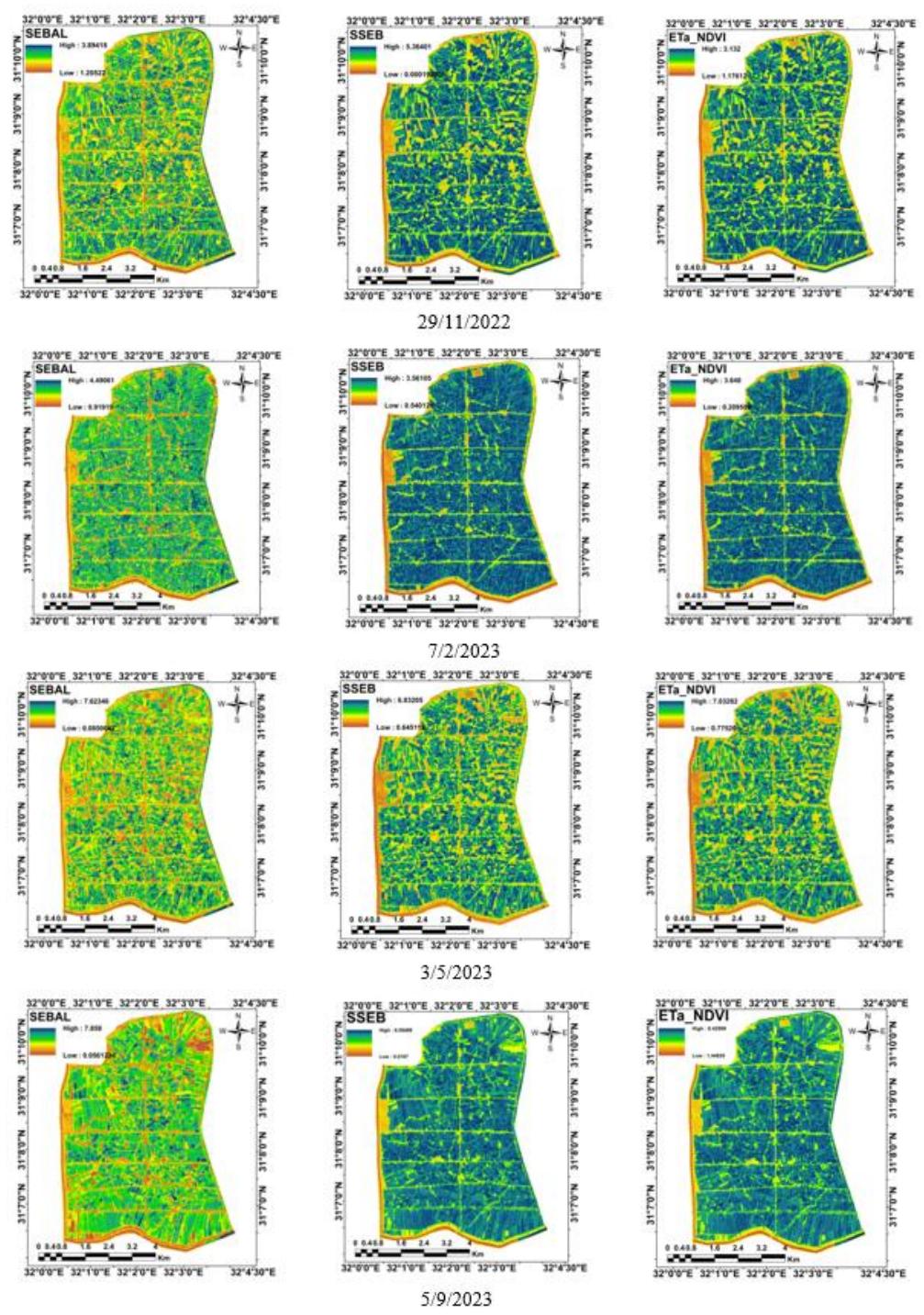


Figure 6. ETa maps estimated from the SEBAL model, SSEB, and ETa\_NDVI.

# 3. Evapotranspiration calculated by the FAO Penman-Monteith method versus SEBAL, SSEB and ETa NDVI

Table 3 shows the average reference evapotranspiration, crop coefficient, and crop evapotranspiration calculated using the FAO Penman-

Monteith method versus actual evapotranspiration from SEBAL, SSEB, and ETa\_NDVI for each winter crop, while Table 4 shows the summer crops. ETc values varied between winter and summer crops and showed close correlation with Kc values. Rice, for example, had the highest water

requirements with ETc of 7.52 mm/day and Kc of 1.10. The lower daily water requirement of wheat was due to a lower crop coefficient Kc (0.74). Results also showed that ETa values estimated from RS models were close to ETc calculated from FAO-PM with small model-specific differences. For example, ETc for wheat was 2.51 mm/day, while estimates were around 2.24-2.43 mm/day depending on the model. In contrast, rice had the ETc at 7.52 mm/day with estimates ranging from 6.79 to 7.34 mm/day.

Regarding the differences between the models, NDVI showed more overestimation compared to the theoretical values. For example, sesame scored 6.11 mm/day compared to 5.07 mm/day, while ETa of other crops like wheat and potato was closer to reference value. As for SEBAL model, most values were close to ETc with differences not exceeding

10%, like corn (5.74 vs. 5.98 mm/day) and sugar beet (3.71 vs. 2.84 mm/day) which reflects the stability of the model. On the other hand, SSEB showed similar behavior to SEBAL with slight tendency towards reduction in certain crops such as wheat (2.41 vs. 2.51 mm/day) and cotton (5.51 vs. 5.13 mm/day, slightly increased).

In general, SEBAL and SSEB methods achieved the best relative accuracy for most crops. The NDVI method had more tendencies to overestimate, particularly for crops with high water requirements such as sesame and rice. This trend is consistent with the research of (Elsayed *et al.*, 2022), who indicated that SEBAL and SSEB achieve better accuracy than vegetation index—based methods in semi-arid regions because they utilize components of surface energy balance.

Table 3. Average Evapotranspiration calculated using the FAO Penman-Monteith method against SEBAL, SSEB and ETa NDVI for the winter season.

	Lu_I \D \ I I I I I I II	c willest beabout				
		FAO-P-M			RS-Methods	
Crop type	ETr(mm/day)	Crop coefficient(Kc)	ETc(mm/day)	ETa_NDVI(mm/day)	SEBAL(mm/day)	SSEB(mm/day)
Wheat	3.63	0.74	2.51	2.43	2.24	2.41
Clover	4.57	0.89	3.81	3.33	3.50	3.45
Potatoes	4.29	0.92	4.15	4.32	4.06	4.13
Sugar beet	4.20	0.84	3.84	3.65	3.71	3.65
Flax	3.47	0.66	2.08	2.46	2.08	2.17
Beans	2.54	0.84	2.06	2.33	2.19	2.18
Onion	3.24	0.90	2.84	3.35	3.10	3.14

Table 4. Average Evapotranspiration calculated using the FAO Penman-Monteith method against SEBAL, SSEB and ETa NDVI for the summer season.

		FAO-P-M-Method			RS-Methods	
Crop type	ETr(mm/day)	Crop coefficient(Kc)	ETc(mm/day)	ETa_NDVI(mm/day)	SEBAL (mm/day)	SSEB(mm/day)
Rice	6.76	1.10	7.52	6.79	7.34	7.28
Maize	6.45	0.89	5.98	5.09	5.74	5.73
Sesame	6.88	0.72	5.07	6.11	5.97	6.10
Sunflower	6.79	0.73	5.08	4.88	5.14	5.12
Cotton	6.30	0.79	5.13	4.89	5.37	5.51

# 4. Evaluation of ETa Estimation Methods Compared to the FAO Method

Figure 7 shows a scatterplot of the estimated ETa value (mm/day) using remote sensing techniques compared to the FAO method during the period 2022-2023 for wheat crops as example for winter crops. The SEBAL model showed a value ranging between 4.60 and 1.20 mm/day, with an average of 2.24 mm/day. The SSEB method showed a value ranging between 5.20 and 1.50 mm/day, with an average of 2.41 mm/day. The ETa\_NDVI model showed that the ETa value ranged between 5.20 and 1.40 mm/day, with an average of 2.43 mm/day.

Additionally, the following figures show that the SEBAL model achieved the highest  $R^2$  accuracy and the lowest RMSE value (0.9642 and 0.24 mm/day, respectively). SSEB ranked second, with  $R^2 = 0.8506$  and RMSE = 0.65 mm/day. On the other hand, the ETa\_NDVI model recorded the lowest  $R^2$  (0.744) and the highest RMSE (0.79 mm/day). These results are consistent with previous studies, where (Bezerra *et al.*, 2015) found higher accuracy and reliability for the SEBAL model than the SSEB model in estimating ETa compared to ground-based FAO-PM measurements. (Elsayed *et al.*, 2022) also demonstrated superiority of the SEBAL model over the SSEB model and the ETa\_NDVI model.

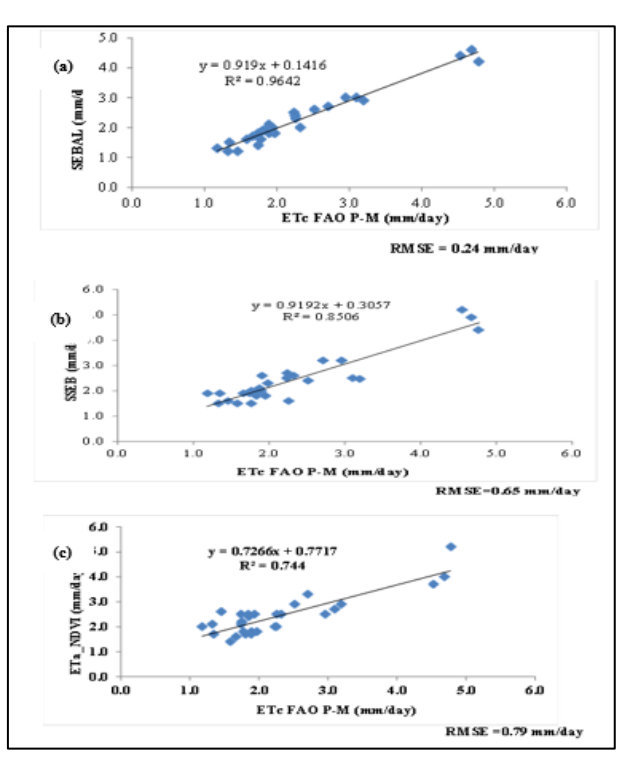


Figure 7. Scatter plot of the estimated ETa value (mm/day) for wheat crop by (a) SEBAL (b) SSEB (c) ETa\_NDVI comparing with the FAO method during 2022-2023.

## 5. Crop type identification

Crop types and their respective areas in hectare were identified using the supervised classification techniques for the winter and summer seasons, as shown in Table 5: Wheat, Clover, Potatoes, Sugar Beet, Flax, Beans, Onion, Rice, Maize, Sesame, Sunflower, and Cotton. In the winter season, wheat and clover were the main crops in this area under flood irrigation, with wheat accounting for 1307.6 hectare and clover for 1569.1 hectare. In the summer season, rice and maize were the main crops, with rice accounting for 1342.1 hectare and maize for 940.0 hectare.

Table 5. Crop type and area (resulting from the classified satellite image).

satemite miage).	
crop types	Area (ha)
Wheat	1307.6
Clover	1569.1
Potatoes	152.8
Sugar beet	83.6
Flax	61.8
Beans	13.1
Onion	102.6
Rice	1342.1
Maize	940.0
Sesame	227.5
Sunflower	419.1
Cotton	278.8

# 6. Comparison of Actual and Theoretical Water Consumption in Irrigation Canals

Table 6 shows the seasonal water requirements, growth period and duration, and irrigation practices for the main crops in the study area (Egypt Delta) during the winter and summer seasons. Wheat, a staple winter crop, requires 6–7 irrigations over a growing period of 150–160 days, with a water requirement of up to 450 mm. Alfalfa exhibits a higher water requirement (approximately 550 mm) due to its need for irrigation after each mowing, with a frequency of 9–14 irrigations and a season length that can extend up to 210 days. Sugar beet requires relatively high water requirements (650

mm) due to its long growing period of 200-180 days. Potatoes, beans, and flax are relatively lower waterconsuming crops compared to beets and alfalfa, despite differences in season length and frequency of irrigation. During the summer season, rice is observed to have the highest water consumption (1045 mm) due to farmers following a continuous flooding system throughout its 120-150-day growth period. This is consistent with the findings of (EA and Abdelkhalek, 2015; Moharram, 2021), who reported that rice cultivation in the Delta is the most water-intensive. Sesame and sunflower crops, on the other hand, exhibit lower water requirements (450-455 mm) and shorter growth periods. Maize and cotton have medium water requirements (575 and 690 mm, respectively) with 6–12 irrigations due to their relatively long growth periods compared to other summer crops.

When evaluating remote sensing methods for estimating actual evapotranspiration rates, the results showed a clear seasonal variation in both the estimated water demand and the estimated quantity between the different methods in terms of accuracy and temporal continuity. The SEBAL model was chosen as an example to be applied to the study area after it was proven to be the best model for estimating actual evapotranspiration. This is consistent with the results of (Elsayed *et al.*, 2022), which confirmed the stability of the SEBAL model under semi-arid conditions.

Figure 8 shows a bar chart of TGIR (in blue) and CAW (in red) values for all months of the year. The estimated CAW remains almost constant across the months, as it depends on the Nile water distribution programs for the various sectors, which are predetermined and do not necessarily change according to changes in actual crop demand. The values of CAW in the table are 88.236, 78.432, 88.236, 84.968, 88.236, 84.968, 88.236, 84.968, 88.236, 98.04, 88.236, 84.968, and 88.236 (x10<sup>5</sup>) m³ for all months from January till December respectively.

Table 6. Seasonal water requirements, growth period and irrigation practices of major crops in the study area (Egypt Delta)SeasonCrop typeNumber of irrigationsPlanting DateHarvest DateDuration(Days)Water Requirement(mm)Wheat6-7Nov-DecApr- May150-160450Clover14-9Oct-NovApr- May120-210550

	wincat	0-7	NOV-DCC	Apr-way	150-100	TJU
	Clover	14-9	Oct-Nov	Apr- May	120-210	550
	Potatoes	6–8	Oct-Dec	Feb-Apr	90-120	500
Winter	Sugar beet	8-10	Sep-Dec	May	180-200	650
	Flax	4–5	Nov-Dec	Apr- May	150-160	430
	Beans	7–8	Oct-Nov	Feb– Apr	120-140	355
	Onion	8-10	Oct –Dec	May	180-210	520
	Rice	10-12( Continuous flooding)	May-Jun	Sep-Oct	120-150	1045
Summer	Maize	6–8	May-Jun	Sep-Oct	~110–130	575
	Sesame	4–5	May-Jun	Sep-Oct	90-120	450
	Sunflower	5-6	Mar–Apr	Jul–Aug	85-105	455
	Cotton	10-12	Mar– May	Sep-Oct	180-190	690

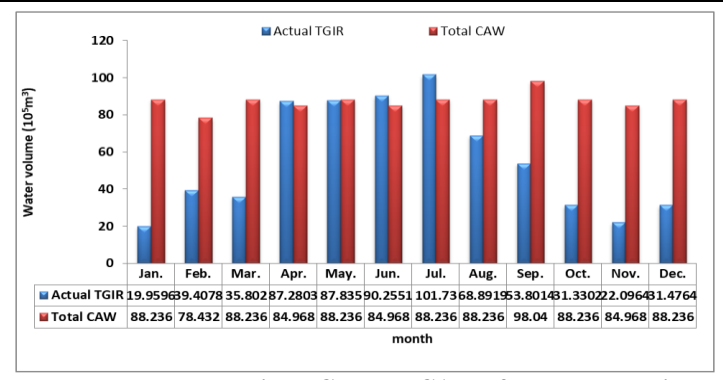


Figure 8. The total water consumption TGIR and CAW of crops planted in the study area.

In contrast, TGIR values showed variability throughout the year and there is a significant difference

between TGIR and CAW during most of the summer months, namely April, May, June, and July. July recorded the highest

TGIR value (10,173,000 m³) compared to CAW value (8,823,600 m³). The values of TGIR in the table are 9.9596, 39.4078, 35.802, 87.2803, 87.835, 0.2551, 101.73, 68.8919, 53.8014, 31.3302, 22.0964, and 31.4764 (x10⁵) m³ respectively. The difference between TGIR and CAW (CAW - TGIR) for all 12 months of the year, January through December, is  $6.828 \times 10^6$ ,  $3.902 \times 10^6$ ,  $5.243 \times 10^6$ ,  $-2.312 \times 10^5$ ,  $4.01 \times 10^4$ ,  $-5.287 \times 10^5$ ,  $-1.3494 \times 10^6$ ,  $1.93441 \times 10^6$ ,  $4.42386 \times 10^6$ ,  $5.69058 \times 10^6$ ,  $6.28716 \times 10^6$ , and  $5.67596 \times 10^6$  m³ respectively. The increase in water consumption during the summer months in general and July in particular is attributed to rising temperatures, due to climate change and solar radiation intensity, and to high levels of Kc of crops, particularly for crops with high water requirements such as rice and maize.

The results suggest that there is a potential water deficit, or increased in water consumption from canals at the expense of other sectors such as industrial sector and domestic use. This could negatively affect crop productivity if effective management measures are not taken, as a result of prevailing agricultural patterns. This could pose a future challenge for water resource management. This has been confirmed in past research (Ramadan *et al.*, 2015).

# **CONCLUSION**

This study draws attention to the challenge of land fragmentation and the prevalence of mixed farming systems in the northern Nile Delta, an area already facing significant water scarcity. The results show that remote sensing models can play an important role in estimating ETa, which is essential for improving irrigation practices and managing limited water resources. Among the models tested, SEBAL delivered the most reliable performance, with strong R<sup>2</sup> values and the lowest RMSE, although it remains computationally demanding. SSEB and ETa NDVI, on the other hand, proved to be practical alternatives because of their simpler data and processing requirements. They can be used in regions where resources or field measurements are limited. These findings confirm that Sentinel-2 imagery combined with remote sensing algorithms can effectively capture spatial and temporal changes in ETa. Looking forward, refining the accuracy of simpler models through methods such as machine learning could make them even more useful. Such improvements would help strengthen precision agriculture and support more sustainable water management in waterstressed regions like the Nile Delta.

# **REFERENCES**

- Abdel Kader, M., Khalifa, H., Sheta, A., & Ibrahim, A. (2015). Evapotranspiration estimation using remote sensing data and some climatic models. *Journal of Soil Sciences and Agricultural Engineering*, 6(11), 1341–1354.
- Abdel-Shafy, H. I., & Aly, R. O. (2002). Water issue in Egypt: Resources, pollution and protection endeavors. Central European Journal of Occupational and Environmental Medicine, 8(1), 3–21.
- Abou El Hassan, W. H. (2011). Impact assessment of long term climate change on reference evapotranspiration and water management in north delta. Journal of Soil Sciences and Agricultural Engineering, 2(6), 623-634.

- Al Zayed, I. S., Elagib, N. A., Ribbe, L., & Heinrich, J. (2016).
  Satellite-based evapotranspiration over Gezira
  Irrigation Scheme, Sudan: A comparative study. Agricultural Water Management, 177, 66-76.
- Alfiky, A., Kaule, G., & Salheen, M. (2012). Agricultural fragmentation of the Nile Delta: A modeling approach to measuring agricultural land deterioration in Egyptian Nile Delta. *Procedia Environmental Sciences*, 14, 79–97. https://doi.org/10.1016/j.proenv.2012.03.008Ali, Y. M., & Khedr, I. S. E. D. (2018). Estimation of water losses through evapotranspiration of aquatic weeds in the Nile River (Case study: Rosetta Branch). *Water Science*, 32(2), 259–275.
- Allen, R. G., Pereira, L. S., Raes, D., & Smith, M. (1998). Crop evapotranspiration-Guidelines for computing crop water requirements-FAO Irrigation and drainage paper 56. *Fao, Rome*, 300(9), D05109.
- Ayyad, S., Al Zayed, I. S., Ha, V. T. T., & Ribbe, L. (2019). The performance of satellite-based actual evapotranspiration products and the assessment of irrigation efficiency in Egypt. *Water*, *11*(9), 1913. https://doi.org/10.3390/w11091913
- Baban, S. M. (2022). The suitability of satellite remote sensing and GIS technologies for mapping, monitoring and managing water resources in the Middle East. *In Satellite monitoring of water resources in the Middle East* (pp. 29–47). Cham: Springer International Publishing. https://doi.org/10.1007/978-3-030-98142-0\_3
- Balataa, I. A., Abdel-Hameed, I. M., & El-Feky, M. M. (2024). THE IMPACT OF CLIMATE CHANGES ON SURFACE WATER RESOURCES: A CASE STUDY OF EGYPT. Sinai Journal of Applied Sciences, 13(1), 73-94.
- Bastiaanssen, W. G. M. (2000). SEBAL-based sensible and latent heat fluxes in the irrigated Gediz Basin, Turkey. *Journal of Hydrology*, 229(1–2), 87–100. https://doi.org/10.1016/S0022-1694(99)00202-4
- Bastiaanssen, W. G. M., Menenti, M., Feddes, R. A., & Holtslag, A. A. M. (1998). A remote sensing surface energy balance algorithm for land (SEBAL): 1. Formulation. *Journal of Hydrology*, 212(1–4), 198–212. https://doi.org/10.1016/S0022-1694(98)00253-4
- Bezerra, B. G., da Silva, B. B., dos Santos, C. A., & Bezerra, J. R. (2015). Actual evapotranspiration estimation using remote sensing: Comparison of SEBAL and SSEB approaches. *Advances in Remote Sensing*, *4*(3), 234–247. https://doi.org/10.4236/ars.2015.43019
- Billah, M., Islam, A. S., Mamoon, W. B., & Rahman, M. R. (2023). Random forest classifications for land use mapping to assess rapid flood damage using Sentinel-1 and Sentinel-2 data. *Remote Sensing Applications: Society and Environment*, 30, 100947. https://doi.org/10.1016/j.rsase.2023.100947
- Chelkeba, B., Feyessa, F. F., & Dibaba, W. T. (2023). Climate change in the upper Awash subbasin and its possible impacts on the stream flow, Oromiyaa, Ethiopia. *Water Science*, 37(1), 179–197. https://doi.org/10.1016/j.wsj.2022.10.002
- Deng, X. P., Shan, L., Zhang, H., & Turner, N. C. (2006). Improving agricultural water use efficiency in arid and semiarid areas of China. *Agricultural Water Management*, 80(1–3), 23–40. https://doi.org/10.1016/j.agwat.2005.07.003

- Döll, P., & Siebert, S. (2002). Global modeling of irrigation water requirements. Water Resources Research, 38(4), 8-1–8-10. https://doi.org/10.1029/2001WR000355
- EA, M., & Abdelkhalek, A. A. (2015). Water requirement components of some egyptian rice varieties in North Nile Delta. Alexandria Science exchange journal, 36(April-June), 131-140.
- Eisenhauer, D. E., Martin, D. L., Heeren, D. M., & Hoffman, G. J. (2021). *Irrigation systems management*. St. Joseph, MI: American Society of Agricultural and Biological Engineers (ASABE).
- Elbeltagi, A., Aslam, M. R., Mokhtar, A., Deb, P., Abubakar, G. A., Kushwaha, N. L., ... & Deng, J. (2021). Spatial and temporal variability analysis of green and blue evapotranspiration of wheat in the Egyptian Nile Delta from 1997 to 2017. Journal of Hydrology, 594, 125662.
- El-Din, M. M. N. (2013). Proposed climate change adaptation strategy for the ministry of water resources & irrigation in Egypt. Joint programme for climate change risk management in Egypt.
- Elhag, M., Psilovikos, A., Manakos, I., & Perakis, K. (2011). Application of the SEBS water balance model in estimating daily evapotranspiration and evaporative fraction from remote sensing data over the Nile Delta. *Water Resources Management*, 25(11), 2731–2742. https://doi.org/10.1007/s11269-011-9831-z
- Elnmer, A., Khadr, M., Kanae, S., & Tawfik, A. (2019). Mapping daily and seasonal evapotranspiration using remote sensing techniques over the Nile Delta. *Agricultural Water Management*, 213, 682–692. https://doi.org/10.1016/j.agwat.2018.11.035
- Elsayed, H., Ibrahim, H., Farag, H., & Sobeih, M. F. (2022). Remote sensing-based techniques for water management in small-scale farms in arid climate. Water Supply, 22(8), 6692-6714.
- El-Shirbeny, M. A., Ali, A. M., Savin, I., Poddubskiy, A., & Dokukin, P. (2021). Agricultural water monitoring for water management under pivot irrigation system using spatial techniques. Earth Systems and Environment, 5(2), 341-351.
- El-Shirbeny, M. A., Ali, A., & Saleh, N. H. (2014). Crop water requirements in Egypt using remote sensing techniques. Journal of Agricultural Chemistry and Environment, 3(2), 57–65.
- El-Shirbeny, M. A., Alsersy, M. A., Saleh, N. H., & Abu-Taleb, K. A. (2015). Changes in irrigation water consumption in the Nile Delta of Egypt assessed by remote sensing. *Arabian Journal of Geosciences*, 8(12), 10509-10519. https://link.springer.com/article/10.1007/s12517-015-2005-2
- Fawzy, H. E. D., Sakr, A., El-Enany, M., & Moghazy, H. M. (2021). Spatiotemporal assessment of actual evapotranspiration using satellite remote sensing technique in the Nile Delta, Egypt. *Alexandria Engineering Journal*, 60(1), 1421–1432.
- Folhes, M. T., Rennó, C. D., & Soares, J. V. (2009). Remote sensing for irrigation water management in the semi-arid Northeast of Brazil. *Agricultural Water Management*, 96(10), 1398–1408.

- Foster, T., Gonçalves, I. Z., Campos, I., Neale, C., & Brozovic, N. (2019). Assessing landscape scale heterogeneity in irrigation water use with remote sensing and in situ monitoring. *Environmental Research Letters*, 14(2), 024004.
- Fritschen, L. J. (1965). Accuracy of evapotranspiration determinations by the Bowen ratio method. Hydrological sciences journal, 10(2), 38-48. https://www.tandfonline.com/doi/abs/10.1080/02626 666509493388
- Immerzeel, W. W., Droogers, P., & Gieske, A. S. M. (2006). *Remote sensing and evapotranspiration mapping: state of the art* (Vol. 39). Wageningen, The Netherlands: FutureWater.
- Ingrao, C., Strippoli, R., Lagioia, G., & Huisingh, D. (2023). Water scarcity in agriculture: An overview of causes, impacts and approaches for reducing the risks. *Heliyon*, 9(8).
- JL, M. (1965). The state and movement of water in living organisms. In 19th Symposia of the Society for Experimental Biology. Cambridge University Press, London, 1965 (pp. 205-234).
- Kang, S., Hao, X., Du, T., Tong, L., Su, X., Lu, H., ... & Ding, R. (2017). Improving agricultural water productivity to ensure food security in China under changing environment: From research to practice. *Agricultural Water Management*, 179, 5–17. https://doi.org/10.1016/j.agwat.2016.05.007
- Lago-Olveira, S., El-Areed, S. R., Moreira, M. T., & González-García, S. (2023). Improving environmental sustainability of agriculture in Egypt through a life-cycle perspective. *Science of the Total Environment*, 890, 164335.
- Li, Z., Liu, X., Ma, T., Kejia, D., Zhou, Q., Yao, B., & Niu, T. (2013). Retrieval of the surface evapotranspiration patterns in the alpine grassland—wetland ecosystem applying SEBAL model in the source region of the Yellow River, China. *Ecological Modelling*, 270, 64–75. https://doi.org/10.1016/j.ecolmodel.2013.08.002
- Losgedaragh, S. Z., & Rahimzadegan, M. (2018). Evaluation of SEBS, SEBAL, and METRIC models in estimation of the evaporation from the freshwater lakes (Case study: Amirkabir Dam, Iran). *Journal of Hydrology*, 561, 523–531. https://doi.org/10.1016/j.jhydrol.2018.04.029
- Ministry of Water Resources and Irrigation (MWRI). (2014). *Water scarcity in Egypt*. Cairo, Egypt: MWRI.
- Moharram, S. H. S. (2021). Evapotranspiration and Irrigation Water requirements in Nile Delta Region. MEJ-Mansoura Engineering Journal, 22(3), 20-33.
- Omar, M. E. M., Abd Elhamid, A. M. I., & Al Zayed, I. S. (2019). Estimating actual evapotranspiration over a large and complex irrigation system of the Nile Delta in Egypt. *International Journal of Recent Technology and Engineering (IJRTE)*, 8(4), 2432–2439.
- Peng, X., He, G., She, W., Zhang, X., Wang, G., Yin, R., & Long, T. (2022). A comparison of random forest algorithm-based forest extraction with GF-1 WFV, Landsat 8 and Sentinel-2 images. *Remote Sensing*, 14(21), 5296. https://doi.org/10.3390/rs14215296

- Penman, H. L. (1948). Natural evaporation from open water, bare soil and grass. *Proceedings of the Royal Society of London. Series A. Mathematical and Physical Sciences*, 193(1032), 120-145.
- Pruitt, W. O., & Angus, D. E. (1960). Large weighing lysimeter for measuring evapotranspiration. https://elibrary.asabe.org/abstract.asp?aid=41105
- Ramadan, M. H., Ibrahim, M. M., & Abd Elwarth, N. A. (2015). Irrigation Water Management In The Nile Delta Using GIS Technology. Misr Journal of Agricultural Engineering, 32(4), 1503-1528.
- Raza, A., Hu, Y., Acharki, S., Buttar, N. A., Ray, R. L., Khaliq, A., Zubair, N., Zubair, M., Syed, N. R., & Elbeltagi, A. (2023). Evapotranspiration importance in water resources management through cutting-edge approaches of remote sensing and machine learning algorithms. In Surface and groundwater resources development and management in semi-arid region: Strategies and solutions for sustainable water management (pp. 1–20). Cham: Springer International Publishing. https://doi.org/10.1007/978-3-031-26500-7\_1
- Rihan, J. I. (2024). Socio-economic challenges and proposed solutions to address the fragmentation of agricultural land holdings in Egypt. *London Journal of Research in Humanities and Social Sciences*, 23(24), 1–17. https://doi.org/10.17472/ljrhss231223
- Roushdi, M. (2024). Investigation the implications of climate change on crop water requirements in Western Nile Delta, Egypt. *Water Science*, *38*(1), 77–91. https://doi.org/10.1016/j.wsj.2023.12.007
- Savoca, M. E., Senay, G. B., Maupin, M. A., Kenny, J. F., Perry, C. A., & Linard, J. I. (2013). Actual evapotranspiration modeling using remotely sensed data in the conterminous United States. *Journal of the American Water Resources Association*, 49(1), 217– 230. https://doi.org/10.1111/jawr.12003
- Sayad, T. A., Ali, A. M., & Kamel, A. M. (2016). Study the impact of climate change on maximum and minimum temperature over Alexandria, Egypt using statistical downscaling model (SDSM). *Glob J Adv Res*, *3*(8), 694-712.

- Sebbar, B. E., Malbéteau, Y., Khabba, S., Bouchet, M., Simonneaux, V., Chehbouni, A., & Merlin, O. (2024).
  Estimating evapotranspiration in mountainous water-limited regions from thermal infrared data: Comparison of two approaches based on energy balance and evaporative fraction. *Remote Sensing of Environment*, 315, 114481.
  https://doi.org/10.1016/j.rse.2023.114481
- Senay, G. B., Leake, S., Nagler, P. L., Artan, G., Dickinson, J., Cordova, J. T., & Glenn, E. P. (2011). Estimating basin scale evapotranspiration (ET) by water balance and remote sensing methods. *Hydrological Processes*, 25(26), 4037-4049.
- Sentelhas, P. C., Gillespie, T. J., & Santos, E. A. (2010). Evaluation of FAO Penman–Monteith and alternative methods for estimating reference evapotranspiration with missing data in Southern Ontario, Canada. *Agricultural Water Management*, *97*(5), 635–644. https://doi.org/10.1016/j.agwat.2009.12.001
- Snyder, R. L. (1992). Equation for evaporation pan to evapotranspiration conversions. *Journal of Irrigation and Drainage Engineering*, 118(6), 977-980. https://ascelibrary.org/doi/abs/10.1061/(ASCE)0733-9437(1992)118:6(977)
- Sun, Z., Wei, B., Su, W., Shen, W., Wang, C., You, D., & Liu, Z. (2011). Evapotranspiration estimation based on the SEBAL model in the Nansi Lake Wetland of China. *Mathematical and Computer Modelling*, 54(3–4), 1086–1092.
  - https://doi.org/10.1016/j.mcm.2010.11.050
- Swinbank, W. C. (1951). The measurement of vertical transfer of heat and water vapor by eddies in the lower atmosphere. *Journal of Atmospheric Sciences*, 8(3), 135-145.
  - https://journals.ametsoc.org/view/journals/atsc/8/3/1 520-0469\_1951\_008\_0135\_tmovto\_2\_0\_co\_2.xml
- Wagle, P., Bhattarai, N., Gowda, P. H., & Kakani, V. G. (2017). Performance of five surface energy balance models for estimating daily evapotranspiration in high biomass sorghum. ISPRS Journal of Photogrammetry and Remote Sensing, 128, 192–203. https://doi.org/10.1016/j.isprsjprs.2017.03.021

# تقتيات الاستشعار عن بعد ونظم المعلومات الجغرافية لإدارة مياه الري في شمال الدلتا بمصر في ظل ظروف ندرة المياه نادر السيد زاحم، محمد ماهر إبراهيم ونادية جمال عبد الفتاح

قسم الهندسة الزراعية، كلية الزراعة، جامعة المنصورة

# الملخص

يُعد الاستشعار عن بُعد ونظم المعلومات الجغرافية فعالين في تقييم استخدام المياه للمحاصيل وتقدير معدلات النبخر والنتج. تهدف هذه الدراسة إلى تحسين تخطيط إدارة المياه في مزارع مختارة من خلال تحديد أفضل تقدير ات النبخر والنتج الفعلي (ETA). يُمثل الموقع المختار مزارع خاصة صغيرة الحجم تقع في شمال دلتا النبل بمصر. باستخدام صور أقمار سنتينل الأوروبية الفترة 2023-2020، فُترت قيم ETa بواسطة (ESBAL)، ومارية المنسطة (SSEB)، وطريقة ولازراعة والماقة السطحية المبسطة (SSEB)، وطريقة هذه النباذج باستخدام نموذج بنمان المعتمد من منظمة الأغذية والزراعة ورنت كفاءة هذه النماذج باستخدام نموذج بنمان المعتمد من منظمة الأغذية والزراعة (FAO-Penman-Monteith) كتموذج مرجعي. وقد قدر نهج بنمان-مونتيث التبخر نتح بـ 2.51، 3.81، 4.15، 80.2، 2.06، 2.08، 2.08، 2.09، كموذج مرجعي. وقد قدر نهج بنمان-مونتيث التبخر نتح بـ 2.51، 3.81، 4.15، 80.2، 2.00، 2.08، 2.08، 4.06، كموذج مرجعي. وقد قدر لنهج بنمان-مونتيث التبخر التربيعي التوالي، في حين أن تقدير التبخر النتح الفعلي (ETa) ملم/يوم على التوالي، في حين أن تقدير التبخر الموسمية المقدرة باستخدام سبيل لهذه المحاصيل كن 2.24، 4.06، 2.08، 2.09، 4.06، 1.06، 2.08، 3.01، 4.06، 3.00، و 1.08 للموسمية المقدرة باستخدام طرائق SEBAL على التوالي، وقد حقق SEBAL على التوالي. تشير كل المؤسم على التوالي. تشير SEBAL على التوالي تموذج SEBAL على التوالي. تشير SEBAL على التوالي تموذج SEBAL على التوالي. تشير SEBAL على التوالية عدال التوالي نموذج SEBAL على التوالي. تشير SEBAL على التوالي. تشير SEBAL على تفوذ كليط الرودة على التوالي تموذج SEBAL على توالي قيمة SEBAL على تفيد SEBAL على تفيد SEBAL على التوالي تشير SEBAL على التوالي تشير SEBAL على التوالي تشير SEBAL على التوالي التوالي المتوالية التفالي التوالي التوالي